Macromolecules

pubs.acs.org/Macromolecules Article

Selective Swelling of Polystyrene (PS)/Poly(dimethylsiloxane) (PDMS) Block Copolymers in Alkanes

Shoutian Qiu, Zhuo Li, Xiangyue Ye, Xiang Ying, Jiemei Zhou, and Yong Wang*

Cite This: *Macromolecules* 2023, 56, 215−225 Read Online

ACCESS | Metrics & More | Article Recommendations | Supporting Information

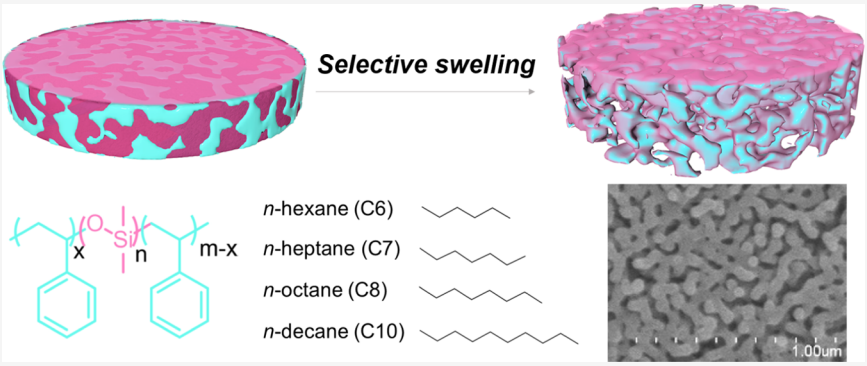

ABSTRACT: Block copolymers (BCPs) containing poly(dimethylsiloxane) (PDMS) blocks have been extensively used as precursors to prepare nanoporous materials with a diversity of compositions and morphologies. However, it remains desirable to facilely and efficiently transform the precursors into porous structures under mild conditions. Herein, we investigate the swelling behaviors of thin films of polystyrene-*block*-poly(dimethylsiloxane)-*block*-polystyrene (PS-*b*-PDMS-*b*-PS, SDS) in linear alkanes and produce well-defined nanoporosities in the SDS films following the mechanism of selective swelling-induced pore generation. Alkanes strongly swell PDMS blocks while slightly swell PS blocks, triggering the cavitation of the PDMS minority phases. The pore sizes as well as the porosities are determined by the interaction between the alkanes and the constituent blocks. Alkanes with lower carbon numbers exhibit a stronger affinity to the copolymer, leading to larger pores. Interestingly, we find that *n*-hexane is able to produce a porosity >30% at room temperature within a duration as short as 1 min. We demonstrate that PDMS, which has a lower surface energy, is enriched on the film surface, thus rendering a strong hydrophobicity to the produced porous SDS films. Ethanol permeation tests demonstrate the interconnected and accessible porosities and tunable flux as well as excellent pressure resistance of the porous SDS films, implying their potential applications as selective membranes in the filtration of organic solvents and oil/water separation.

1. INTRODUCTION

Block copolymers (BCPs), composed of two or more chemically distinct homopolymer chains that are covalently tethered together, tend to microphase-separate as a result of thermodynamic incompatibility between constituent blocks.[1−4] Microphase separation of BCPs leads to well-defined periodical structures with feature sizes typically ranging from ∼5 to 50 nm. Consequently, BCPs have been attracting increasing interest in many fields such as thermoplastic elastomers, microelectronics, optoelectronics, biomedicines, catalysis, and separation.[5]

Thousands of BCPs are expected to be theoretically available; however, only dozens of them have been synthesized and used in different applications.[5−7] Among them, BCPs containing the poly(dimethylsiloxane) (PDMS) blocks, either in the form of diblock or triblock, are a unique type of BCPs and have gained extensive attention in the past decades for multiple reasons. First, PDMS-containing BCPs, e.g., polystyrene (PS)-*block*-PDMS (PS-*b*-PDMS), one of the most commonly used BCPs, are prone to microphase-separate even with very low molecular weights because of the high Flory−Huggins interaction parameter (χ) between PS and PDMS. This enables the easy and fast formation of highly ordered morphologies with narrow interfaces between the microdomains.[8,9] Second, PDMS, containing both inorganic Si element and organic methyl groups, is a borderline polymer between organic and inorganic materials;[10] therefore, PDMS-containing BCPs are likely to be transformed into an organic−

Received: September 13, 2022
Revised: November 20, 2022
Published: December 26, 2022

https://doi.org/10.1021/acs.macromol.2c01903
Macromolecules 2023, 56, 215−225

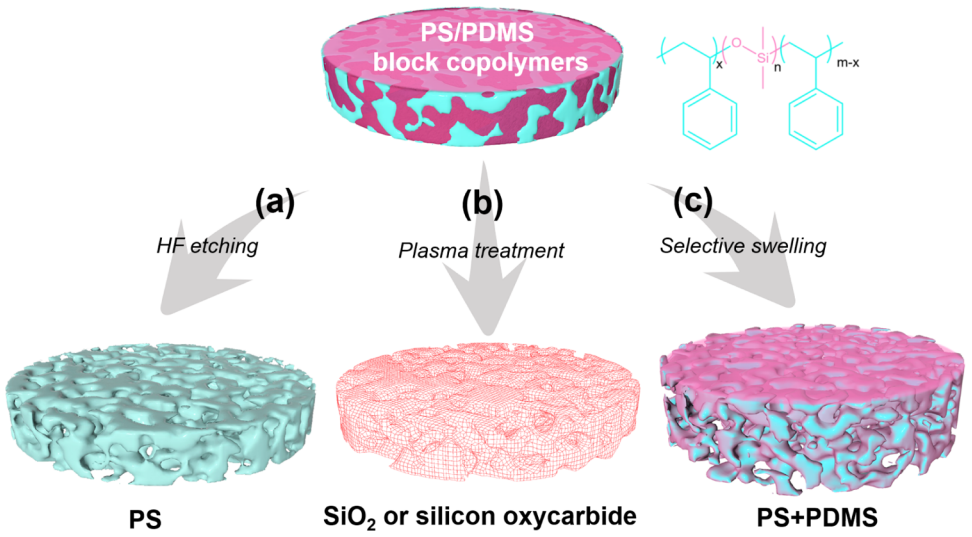

Figure 1. Schematic diagram of the preparation of nanoporous films from PS/PDMS block copolymers using different strategies: (a) HF etching, (b) plasma treatment, and (c) selective swelling.

inorganic hybrid or purely inorganic materials. Third, PDMS can be easily covalently bonded with a number of other polymers such as PS, polybutadiene (PB), polyisoprene (PI), polyethylene, polycaprolactone, poly(methyl methacrylate), and polyamide to form BCPs through various synthetic strategies including anionic polymerization, ring-opening polymerization (ROP), step-growth polymerization, and atom transfer radical polymerization (ATRP).[11,12] Last but not least, unlike the brittleness of many commonly used BCPs, PDMS-containing BCPs may exhibit excellent flexibility and improved mechanical properties because of the rubbery nature of PDMS under ambient conditions.[10]

The main application of PDMS-containing BCPs is to use them as precursors to prepare nanoporous materials including monoliths and thin films or membranes by converting some discrete components in the phase-separated BCPs into voids.[13] The phase separation behaviors of PDMS-containing BCPs can be regulated to produce diverse morphologies such as cylinders oriented in the perpendicular or parallel direction.[14−17] The phase-separated BCPs are then used to generate arrays of discrete nano-objects or nanoporous scaffolds by selective removal of the PDMS blocks or all of the organic moieties in the BCPs.[18,19] Some researchers selectively etched away the PDMS domains by soaking in hydrofluoric acid (HF), and the continuous phases composed of non-PDMS blocks, typically PS, cross-linked PB, or PI are left behind, producing nanoporous films or monoliths with interconnected porosities initially occupied by the PDMS phases (Figure 1a).[20−28] Alternatively, some others prefer to use plasma treatment to decompose the PS blocks and the organic moieties in the PDMS blocks, thus producing nanoporous silicon oxide or silicon oxycarbide (Figure 1b).[29−33] However, removal of the PDMS blocks from the BCPs requires harsh conditions, for instance, highly toxic HF and high-energy plasma etching, making the pore-forming process tedious, complicated, and less efficient. Even worse, the pores are produced at the expense of the degradation of PDMS or its organic moieties, which not only weakens the mechanical robustness of the eventually produced porous materials but also results in troublesome byproducts. Therefore, it is highly desired for nondestructive strategies to prepare nanoporous structures from PDMS-containing BCPs independent of the chemistry of PDMS.

Selective swelling, an emerging pore-making method, has shown important advantages in the preparation of nanoporosities in BCPs for its extreme simplicity, high efficiency, and nondestructive nature.[34−37] The principle of selective swelling is to transform the dispersed phases composed by the minority blocks in BCPs into empty volumes (i.e., pores) by utilizing the difference in the swelling tendency between the minority block and the majority block in selective solvents. This strategy does not rely on the sacrifice of any component or phase of the BCPs to produce pores, and the BCPs remain chemically intact after pore formation. Moreover, after swelling, the minority blocks migrate to the surface including pore walls, forming an additional layer uniformly lined along the entire surfaces of the BCPs.[38] To date, a number of BCPs, mainly including polystyrene-*block*-poly(2-vinylpyridine) (PS-*b*-P2VP),[37,39] polystyrene-*block*-poly(4-pyridine),[34] polystyrene-*block*-poly(ethylene oxide),[40,41] polystyrene-*block*-poly(methyl methacrylate),[42] poly(2-(dimethylamino) ethyl methacrylate)-*block*-polystyrene (PDMAEMA-*b*-PS),[43,44] and polysulfone-*block*-poly(ethylene glycol) (PSF-*b*-PEG),[45] have been used to produce nanoporous structures in the form of one-dimensional (1D) nanofibers, two-dimensional (2D) thin films, and three-dimensional (3D) monoliths by the process of selective swelling-induced pore generation. We note that almost all of the previously investigated BCPs capable of pore formation by selective swelling contain minority blocks of polar or even hydrophilic polymers such as P2VP and PEO, and consequently, polar solvents such as ethanol are required to use as the swelling agent to enable the strong swelling of the polar minority blocks. Thus-produced porous materials, for example, membranes, typically exhibit strong surface hydrophilicity and are particularly suitable for usage in aqueous systems.[36] However, in some particular applications such as membrane distillation and the filtration of organic solvents, porous membranes with strong hydrophobicity are required. Moreover, the swelling behaviors of BCPs composed of two or more nonpolar blocks in nonpolar but selective solvents remain to be elucidated, and selective swelling-induced pore generation of strongly hydrophobic BCPs is to be explored.

https://doi.org/10.1021/acs.macromol.2c01903
Macromolecules 2023, 56, 215−225

Considering the large difference in surface energy between PS and PDMS ($\gamma_{PS} \approx 40.7$ mN·m^{-1} and $\gamma_{PDMS} \approx 20.4$ mN·m^{-1}) and a relatively large interaction parameter between them ($\chi = 0.14$),[46] we expect that there is a possibility to find some solvents which slightly swell PS but strongly swell PDMS, thus triggering selective swelling-induced pore generation of BCPs of PS and PDMS and producing nanoporous films with PS as the skeleton and PDMS lined along the pores. Thus-prepared porous films are expected to display hydrophobic surfaces as the PDMS block is inclined to migrate to the film surface for its low surface energy. In this work, we synthesize triblock copolymers of PS and PDMS, i.e., polystyrene-*block*-poly(dimethylsiloxane)-*block*-polystyrene (PS-*b*-PDMS-*b*-PS, abbreviated as SDS below), and treat the SDS films in alkanes with different carbon numbers. We demonstrate the feasibility of selective swelling-induced pore generation of SDS to prepare nanoporous membranes with strong inherent surface hydrophobicity and reveal the pore-forming mechanism and swelling behaviors of SDS films under various swelling conditions (Figure 1c). We discover that low-carbon alkanes are capable of fast activating SDS films under ambient conditions (e.g., room temperature), and thus-obtained hydrophobic porous films are expected to show potential applications in the filtration of organic solvents and oil/water separations.

2. EXPERIMENTAL SECTION

2.1. Materials. Poly(dimethylsiloxane) with aminopropyl as the end group (bis(aminopropyl)-functional PDMS, M_n = ∼10 kDa) and styrene (≥99.9%) were supplied by Energy Chemical. SDS (M_n = 6.1 kDa, PDI = 2.48) with a PDMS percentage of 15.2 wt % (calculated by ^{1}H NMR) was synthesized from the styrene monomer and PDMS macroinitiator. Details of the synthesis and characterization of SDS are given in the Supporting Information (Figures S1 and S2). Anhydrous tetrahydrofuran (≥99.9%), *n*-heptane (≥99.0%), and *n*-decane (≥99.0%) were purchased from Aladdin. *n*-hexane (≥95%) was obtained from Sigma-Aldrich, while *n*-octane (≥98.5%) was supplied by Macklin. Other chemicals including anhydrous ethanol (≥99.8%) and chloroform (≥99.0%) were provided by local suppliers. Hydrophilic polyvinylidenefluoride (PVDF) microfiltration membranes with a mean pore diameter of 220 nm were obtained from Millipore and used as substrates for the preparation of composite SDS membranes. All of the chemicals were used without further purification. Silicon wafer was ultrasonically treated before use. Deionized water (8-20 μS·cm^{-1}) was homemade and used throughout this work.

2.2. Selective Swelling of SDS Thin Films. SDS was dissolved in chloroform to prepare the film-forming solution with a concentration of 1.5 wt %. The solution was then filtrated through PTFE filters three times to remove any insoluble impurities before use. Subsequently, the SDS solution was spin-coated on cleaned silicon wafers at 2000 rpm for 30 s. As-coated SDS films were then equilibrated at 25 °C for at least 12 h before use. The SDS films were soaked in selective solvents (*n*-hexane (C6), *n*-heptane (C7), *n*-octane (C8), and *n*-decane (C10)) at fixed temperatures for preset durations to perform selective swelling. After being withdrawn from selective solvents, the films were allowed to dry at ambient conditions.

2.3. Preparation of SDS Composite Membranes. We prepared composite membranes by spin-coating SDS solutions on the surface of PVDF substrates, followed by selective swelling. PVDF substrates were first filled with water by immersing them in deionized water for 1 h to prevent the SDS solution from leaking downward in the process of spin-coating. After removing from water, the water-filled PVDF substrate was placed on the surface of the glass slide, and redundant water on the surface was then carefully wiped with a soft paper as fast as possible. The SDS solution was then spin-coated (2000 rpm, 30 s) on PVDF substrates immediately, followed by equilibration at 25 °C for at least 12 h to evaporate all of the volatile phases (including residue chloroform and deionized water) involved in the spin-coating process. Afterward, selective swelling was performed at a preset temperature for desired durations to produce pores in the coating SDS layers, thus producing composite membranes with the nanoporous SDS as the separation layers.

2.4. Characterizations. The surface and cross-sectional morphologies of SDS films subjected to various treatments were probed by scanning electron microscopy (SEM, Hitachi S4800) at an accelerating voltage of 3 kV. The cross sections of samples were obtained by freeze fracturing in liquid nitrogen. All of the samples were sputter-coated with a thin layer of platinum under vacuum at a sputtering current of 15 mA for 30 s to enhance the conductivity.

We used two parameters to characterize the porous state of the films. One is volume porosity considering the percentage of volumes of all the pores in the entire film, and the other is surface porosity considering only the percentage of pore openings on the film surface. Volume porosity is defined by the volume increase of the BCP films after swelling. Volume expansion of BCP films induced by selective swelling occurs only in the *Z* direction, and the lateral size of the films will not change during swelling as they tightly adhere to the substrates. Therefore, volume porosity can be easily determined by comparing the thickness of the SDS films before and after swelling. The thickness of SDS films deposited on silicon wafers were measured by a spectroscopic ellipsometer (Complete EASE M-2000U, J. A. Woollam) with an incidence angle of 70°. The film thickness of each sample was tested before and after swelling separately to calculate the volume porosity of each system, at least three samples were tested and the mean value was used. The surface porosity is estimated by determining the percentages of pore openings on the surface SEM images with ImageJ software.

The static water contact angles (WCAs) were recorded by a contact angle goniometer (Dropmeter A100, Maist) to evaluate the surface properties of SDS films. At least three positions were tested for each film and the average value was reported. The surface elemental analysis and chemical compositions of the films before and after swelling were investigated by X-ray photoelectron spectroscopy (XPS, Thermo Fisher Nexsa) with 150 W monochromatic Al Kα excitation ($h\nu$ = 1486.7 eV) on a spot size of 500 μm. The surface roughness of SDS films were performed on atomic force microscopy (AFM, BRUKER Dimension Icon) at the noncontact mode. The scan area was set as 5 μm × 5 μm.

2.5. Filtration Tests. Ethanol permeances of SDS composite membranes were tested on a dead-end filtration module (Amicon8003, Millipore) at room temperature. Before the test, the membrane with a diameter of 25 mm was prepressed by ethanol at 0.5 bar for 10 min to obtain stable permeance. The ethanol permeance tests were then performed at a pressure of 0.5 bar. The pressure resistance of the membranes was characterized by measuring the flux of the SDS membranes under increased pressures varied from 0.5 to 6.0 bar. All of the tests were carried out continuously for 5 min under each pressure.

3. RESULTS AND DISCUSSION

3.1. Effect of Swelling Solvents and Swelling Durations. According to the principle of selective swelling-induced pore generation,[34,47] the suitable swelling solvent should have a strong affinity with the minority block (PDMS) and simultaneously enhance the mobility of the majority block (PS) to a moderate degree under the swelling conditions so as to ensure that PDMS can effectively absorb the swelling solvent and the PS phase will undergo plastic deformation. By carefully considering the interactions between the swelling solvents and the two blocks, as well as taking the cost of the swelling process (including the type of the swelling solvent and the swelling temperature and duration) into account, we selected linear alkanes including *n*-hexane (C6), *n*-heptane (C7), *n*-octane (C8), and *n*-decane (C10), as the selective

https://doi.org/10.1021/acs.macromol.2c01903
Macromolecules 2023, 56, 215−225

solvents. Unlike the polar solvents used before,[36] linear alkanes are commonly used nonpolar solvents, which may lead to different swelling behaviors unexpected in the cases of swelling of BCPs by polar solvents.

To better understand the pore-forming process of SDS films, we tracked the change in the volume porosity of the films with soaking durations by observing the increase in film thickness before and after swelling. As is illustrated in Figure 2, SDS films

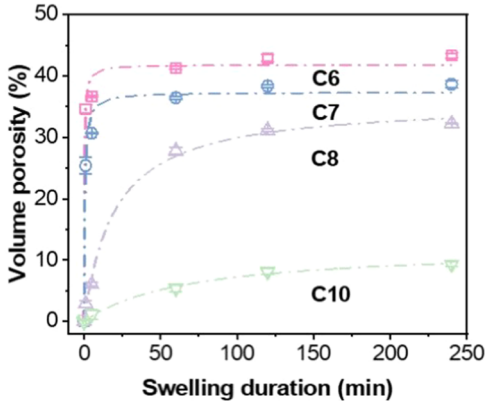

Figure 2. Evolution of the volume porosity of SDS films with swelling duration subjected to swelling in different alkanes at 25 °C. Dashed lines are the corresponding fitting curves following the pseudo-second-order kinetics equation.

obtained varied volume porosities significantly dependent on the used alkanes as well as the swelling durations. We performed curve fitting to the change of volume porosities with swelling time for different alkanes and found that the data could fit in a pseudo-second-order kinetics equation with the correlation coefficient (R) close to or better than 0.99

$$\mathrm{VP} = \frac{A \times k \times t}{1 + k \times t} \tag{1}$$

where VP (%) represents the volume porosity of SDS films after swelling, t (min) is the swelling time, and A and k are both kinetic constants depending on the interactions between these alkanes and the two blocks of SDS.

The pore formation in SDS films is caused by the different swelling degrees of PS and PDMS in alkanes, and the swelling degree is mainly determined by the interaction between the swelling solvent and the constituent blocks. From Figure 2, we can see that the carbon number of alkanes greatly influences the swelling degree, and alkanes with smaller carbon numbers exhibit higher swelling efficiency. Specifically, swelling in C10 and C8 for 1 min could hardly generate pores as negligible porosities of 0.3 and 2.9% were produced, respectively. In contrast, the volume porosity swelling for 1 min was increased to 25.4% when swelling in C7 and further reached 34.6% when the selective solvent was changed to C6. It has also been observed that the volume porosity always reaches a stable value after a certain swelling duration, which is considered as the arrival of the swelling equilibrium. For example, the volume porosity of the film swelling-treated in C6 for 1 min was dramatically increased to 34.6% but was only modestly increased to 41.3% after swelling for 1 h. Afterward, the volume porosity almost remained unchanged with further extended swelling durations. Typically, the swelling equilibrium was close to being reached after swelling for 1 h for all of the cases using different alkanes as the swelling solvent; therefore, 1 h was fixed as the swelling duration in our subsequent investigations. It is worth noting that under the equilibrium swelling conditions, the volume porosity of SDS films depends heavily on the carbon number of the alkane swelling solvents. With increasing carbon numbers of alkanes, the volume porosity gradually declined. After swelling in C6, C7, C8, and C10 for 4 h, the volume porosities of the films were 43.3, 38.6, 32.2, and 9.3%, respectively. This should be attributed to the discrepancy in the interactions between these alkanes and the two blocks of SDS. Typically, the interaction parameter between a solvent and a polymer can be estimated by the following equation

$$\chi_{\mathrm{polymer-solvent}} = \frac{V \times [(\delta_{\mathrm{d}}^{\mathrm{p}} - \delta_{\mathrm{d}}^{\mathrm{s}})^2 + 0.25(\delta_{\mathrm{p}}^{\mathrm{p}} - \delta_{\mathrm{p}}^{\mathrm{s}})^2 + 0.25(\delta_{\mathrm{h}}^{\mathrm{p}} - \delta_{\mathrm{h}}^{\mathrm{s}})^2]}{R \times T} \tag{2}$$

where $\chi_{\mathrm{polymer-solvent}}$ represents the Flory–Huggins interaction parameter; V (cc·mol^{-1}), R (J·mol^{-1}·K^{-1}), and T (K) are the molar volume, gas constant, and the absolute temperature, respectively; $\delta_{\mathrm{d}}^{\mathrm{s}}$, $\delta_{\mathrm{p}}^{\mathrm{s}}$, and $\delta_{\mathrm{h}}^{\mathrm{s}}$ (MPa$^{1/2}$) are the dispersion, polar, and hydrogen-bonding components of Hansen solubility parameter for the solvent, respectively; and $\delta_{\mathrm{d}}^{\mathrm{p}}$, $\delta_{\mathrm{p}}^{\mathrm{p}}$, and $\delta_{\mathrm{h}}^{\mathrm{p}}$ are the corresponding Hansen solubility parameters of the polymer. The $\delta_{\mathrm{d}}^{\mathrm{p}}$, $\delta_{\mathrm{p}}^{\mathrm{p}}$, and $\delta_{\mathrm{h}}^{\mathrm{p}}$ values are 21.8, 5.8, and 4.3 for PS, while 14.61, 4.9, and 0 for PDMS, respectively.[48,49] Other parameters and the calculated interaction parameters are listed in Table 1. $\delta_{\mathrm{p}}^{\mathrm{s}}$ and $\delta_{\mathrm{h}}^{\mathrm{s}}$ of alkanes are zero and not listed in Table 1.[50]

As clearly shown in Table 1, C6 shows the smallest interaction parameters with both blocks of SDS (1.10 with PS and 0.32 with PDMS), thus endowing the PS blocks with the strongest enhancement in mobility and plastic deformation during swelling. Therefore, films swelling-treated in C6 under the equilibrium swelling conditions displayed the highest volume porosity as described above. Moreover, with the

Table 1. Solubility Parameters,[50] the Molar Volume of Solvents, and the Calculated Polymer–Solvent Interaction Parameters Involved in This Study

solvent	temperature (°C)	$\delta_{\mathrm{d}}^{\mathrm{s}}$ (MPa$^{1/2}$)	V (cm^3·mol^{-1})	$\chi_{\mathrm{PS-solvent}}$	$\chi_{\mathrm{PDMS-solvent}}$
n-hexane (C6)	25	14.9	131.6	1.10	0.32
n-heptane (C7)	25	15.3	147.4	1.12	0.39
n-octane (C8)	25	15.5	163.5	1.18	0.45
	35			1.14	0.43
	45			1.10	0.42
	55			1.07	0.41
n-decane (C10)	25	15.7	195.9	1.35	0.57

https://doi.org/10.1021/acs.macromol.2c01903
Macromolecules 2023, 56, 215–225

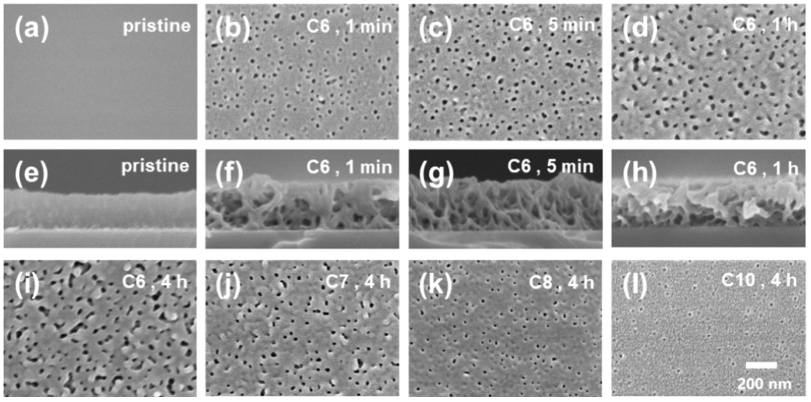

Figure 3. SEM images of SDS films subjected to swelling in different alkanes at 25 °C for various durations. Panels (a−d) and (i−l) are surface images, while panels (e−h) are cross-sectional images. All of the images have the same magnification and the scale bar is given in (l).

increase in the carbon number of the alkanes, the interaction between alkanes and PS blocks was weakened, leading to less enhancement in the segmental mobility of PS and, consequently, the progressive decline of the volume porosity. Moreover, the swelling process of SDS films in linear alkanes, especially in C6, can be accomplished rapidly, even at room temperature. This is a very quick pore-forming process, as approximately 80% of the equilibrated volume porosity can be obtained within 1 min. This is because (1) there is a strong affinity between C6 and PDMS blocks and (2) the segment mobility of PS comprised the matrix of SDS films is simultaneously enhanced to an appreciable extent in C6.[45]

We used SEM to track the morphology evolution of SDS films subjected to swelling in different alkanes. As depicted in Figure 3a,e, the pristine SDS film before swelling exhibited a thickness of ∼200 nm, which is very close to the value measured by a spectroscopic ellipsometer. Moreover, the surface and the cross-section were both dense and pore-free, indicating that no defects occurred in the film coating process. Besides, all of the SDS films before swelling showed almost the same thickness. After exposure to C6 for a short duration (1 min), circular holes with a diameter of dozens of nm appeared on the film surface (Figure 3b). Moreover, the film thickness increased and perforating pore channels were formed (Figure 3f). The presence of pores in the surface and the cross section was in accordance with the evolution of volume porosity shown in Figure 2. Same as the change in volume porosity discussed above, the film thickness was only slightly increased with the swelling duration prolonged to 5 min and 1 h (Figure 3g,h). Besides, the film thickness after swelling in C6 for 1 min, 5 min, and 1 h was ∼300, ∼310, and ∼330 nm, respectively. By comparing the film thickness before and after swelling in SEM images, the volume of pores that open up because of the selective swelling was ∼33.4, ∼35.5, and ∼39.4%, which are very close to the volume porosities discussed above. Therefore, volume porosity is a reasonable parameter to evaluate the pore opening of porous films.

By extending the swelling duration, although the volume porosity did not evidently rise sharply, the surface porosity and the pore size kept continuously increasing, implying that prolonged swelling duration can further increase the pore size and pore connectivity. As can be seen from Figures 3 and S4a, after swelling in C6 for 1 min, only isolated circular pores could be observed on the film surface, corresponding to a low surface porosity of 3.6%. However, when the swelling duration was prolonged to 1 h, the circular pores on the film surface were enlarged and some coalesced with adjacent pores, forming interconnected pores. Consequently, a bicontinuous structure was generated in the SDS film. The surface porosity of the SDS film swelling-treated for 1 h was increased to 8.7%. Further extending the swelling time to 4 h, the volume porosity (43.3%) was almost unchanged, but the surface porosity increased from 8.7 to 9.8% (Figure S4c,d). The surface porosity further increased with extending swelling durations, and more surface pores coalesced, resulting in a pronounced interconnected porous morphology.

Considering the strong interaction between the PDMS block and C6, we further check the structural stability of SDS films subjected to relatively long swelling durations. As clearly shown in Figure S3a, films swelling-treated for 1 day and 7 days gave similar volume porosities to that of the film swelling-treated for 4 h; only slightly enlarged pores and surface porosities were observed (Figure S3b,c). Notably, even after swelling for 7 days, the SDS film still maintained a stable, porous structure, implying that long-term swelling, even for one week, did not damage the structure of the produced porous films. Moreover, we also understand that once the equilibrium swelling is reached, prolonged swelling has little effect on the volume porosity but slightly enlarges the pore size and, consequently, the surface porosity.

However, for the alkanes with larger carbon numbers, the swelling effect was retrogressed as a result of the weakened interaction between alkanes with PDMS and PS. For example, at the same swelling duration of 4 h, the volume porosity of the SDS film swelling in C7 was decreased to 38.6%, while the surface porosity declined to 4.1% (Figure S4g). Meanwhile, the pores were mainly present in the isolated stated and coalesced pores rarely appeared (Figure 3j). When the swelling solvent was changed to C8, only circular pores appeared on the film surface, although the volume porosity still reached 32.3%. Moreover, the pores were sparsely presented on the film surface with a very low surface porosity of 1.3% (Figures 3k and S4h). When C10 was used as the swelling agent, the film thickness was only increased by 9.3% as a result of the weakest interaction between C10 and the SDS (0.57 with PDMS and 1.35 with PS), and very few isolated pores appeared on the film surface (Figure 3l).

3.2. Effect of Swelling Temperature. In previous works, the swelling of amphiphilic BCPs was generally carried out at elevated temperatures for the sake of enhanced interactions between the swelling solvents and the BCPs.[47] Presently, we expect a stronger swelling effect can also be achieved by

https://doi.org/10.1021/acs.macromol.2c01903
Macromolecules 2023, 56, 215−225

increasing the swelling temperature. Because the interaction of C8 with SDS was relatively weak (1.18 with PS and 0.45 with PDMS), the ultimate volume porosity was less than 30% at 25 °C, allowing a relatively wide window to see the effect of swelling temperature. Thus, we adopted C8 as the swelling solvent to investigate the porosity and morphology changes of SDS films within the temperature range of 25−55 °C. As shown in Figure 4, when the swelling temperature increased to

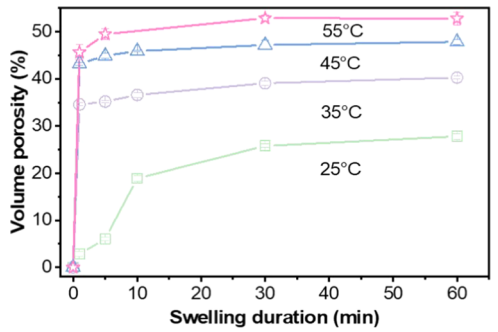

Figure 4. Changes of volume porosity with swelling duration of SDS films subjected to swelling at different swelling temperatures.

35 °C or above, the volume porosity of the films increased dramatically because of significantly enhanced interactions of C8 with PS (the interaction parameter between C8 and PS descended from 1.14 at 35 °C to 1.07 at 55 °C, Table 1). As a result, the equilibrium swelling condition was nearly achieved within 1 min, while the volume porosity was rapidly increased to 34.6% at a swelling temperature of 35 °C; however, the volume porosity was only 40.3% when the swelling duration was extended to 1 h. This confirms our previous finding that under the equilibrium swelling condition, prolonging swelling only increases the surface porosity and the pore size but hardly influences the volume porosity. It is worth noting that the volume porosity of the SDS films under equilibrium swelling conditions was significantly increased with rising swelling temperatures. Under the equilibrium swelling condition at 25, 35, 45, and 55 °C, the volume porosities of the SDS films were 27.8, 40.3, 47.9, and 52.8%, respectively. The solubility parameter of PS with C8 at 45 °C is 1.10, which is close to the interaction parameter of PS with C6 (1.10) at 25 °C; therefore, their volume porosity was also close (47.9 vs 41.3%). That is, increasing the swelling temperature and changing better swelling solvent are sometimes equivalent to improving the interactions between solvent and BCP blocks (i.e. lowing the interaction parameters), and eventually promoting the volume porosity of the produced porous SDS films.

The surface morphologies of films after swelling in C8 for 1 h at different temperatures are shown in Figure 5. It is clear that at the swelling temperature of 25 °C, circular pores isolated from each other were present on the film surface, giving a surface porosity of only 0.6%. When the swelling temperature was increased to 35 °C, the adjacent pores started to coalesce, forming interconnected pores. The surface porosity also increased to 9.8%, while the volume porosity changed to 27.8%. When the temperature was raised to 45 °C, because of the interaction parameters close to the case of C6 at 25 °C, similar volume porosity was achieved. However, the surface porosity (∼16.7%) was much higher than that in C6 at 25 °C (∼8.7%). This may be due to the smaller interaction between PDMS and the solvent (0.32 for C8 at 45 °C and 0.42 for C6 at 25 °C).

Further increasing the swelling temperature to 55 °C, an interconnected bicontinuous morphology was observed (Figure 5d). The surface porosity was as high as 27.2%. Besides, the film swelling in C8 at 55 °C gave the highest volume porosity (52.8%). Under this condition, the film still maintained a porous structure (Figure 5d,h). Specifically, the evolution of surface morphologies with the swelling duration at different temperatures is shown in Figure S5. Interestingly from Figure 5i, the volume porosity was always higher than the surface porosity under the same swelling conditions. We believe that during swelling, the volume porosity initially increases rapidly, approaching a constant value, and then the swelling still goes on and the PDMS blocks continue to migrate to the film's surface, leading to the shrinkage of pore openings on the surface and consequently a difference between volume porosity and surface porosity. To be specific, volume

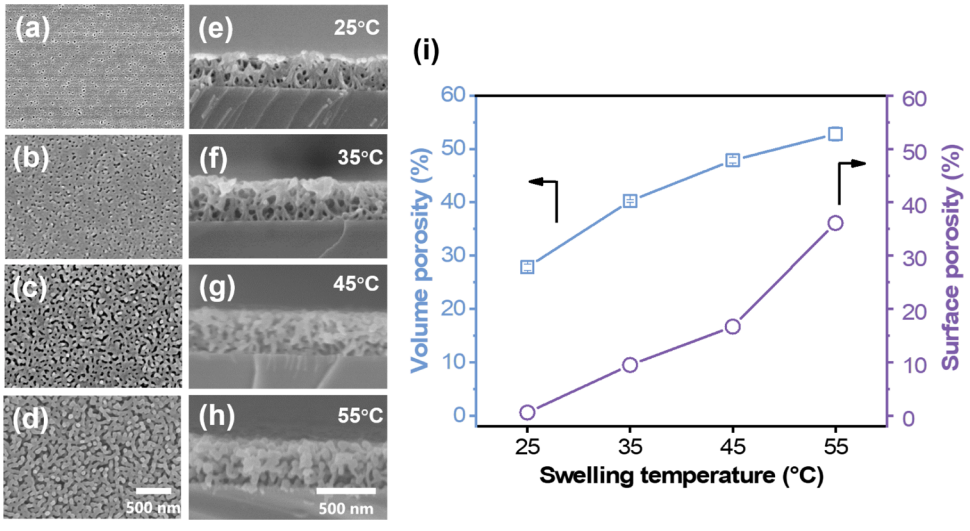

Figure 5. (a−d) Surface and (e−h) cross-sectional SEM images of SDS films subjected to swelling in C8 at varied temperatures for 1 h, (i) evolution of the volume porosity and surface porosity with swelling temperatures subjected to swelling in C8 for 1 h. Panels (a−d) and (e−h) separately have the same magnification and the scale bar is given in panels (d) and (h), respectively.

https://doi.org/10.1021/acs.macromol.2c01903
Macromolecules 2023, 56, 215−225

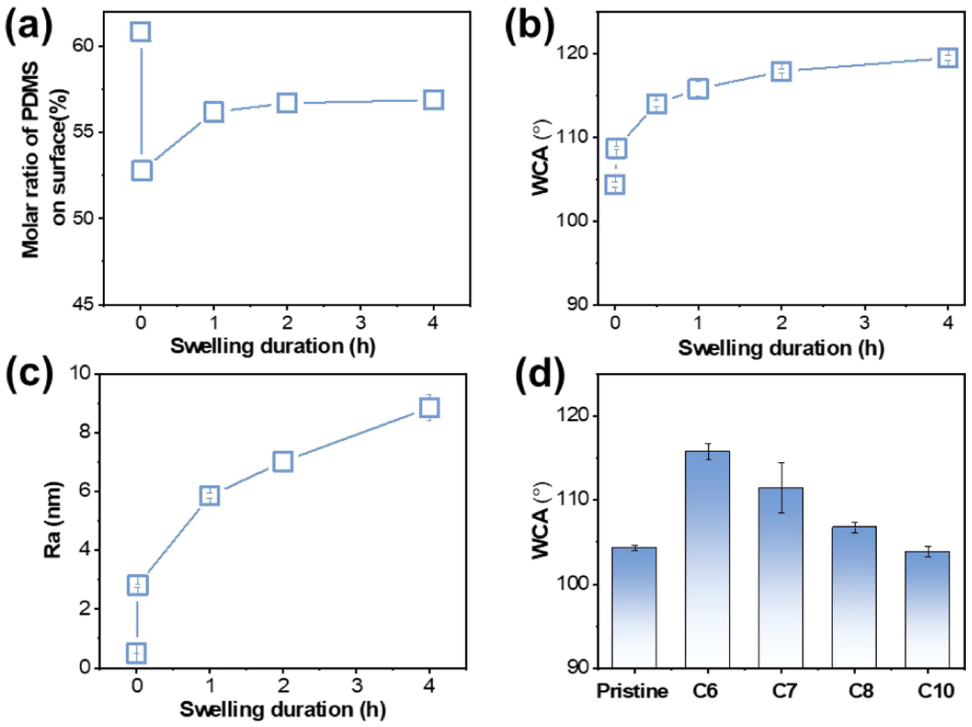

Figure 6. (a) PDMS molar ratio on the surface, (b) the water contact angle, (c) the surface roughness of SDS films subjected to swelling in C6 at 25 °C for various durations, and (d) the water contact angle of SDS films subjected to swelling in different alkanes at 25 °C for 1 h.

porosity represents the expansion degree of film thickness, which is dependent on the character of the film matrix. However, surface porosity is estimated from the surface openings observed by SEM imaging and is more related to the PDMS phase on the film surface. Typically, the difference became smaller on account of the stronger swelling kinetics under elevated swelling temperatures. As shown in Figure 5i, for the SDS film swelling in C8 for 1 h, its volume porosity reached 27.8% while its surface pore was as low as 0.6%. Additionally, the pores on the surface (Figure 5a) were clearly smaller than those in the interior (Figure 5b).

To summarize, for a given SDS, once the swelling parameters (i.e., swelling temperature and swelling solvent) were fixed, the volume porosity would finally reach a constant value under the equilibrium swelling conditions. However, prolonging the swelling duration may continuously promote surface porosity and enlarge the pore sizes. Therefore, we can obtain porous films with desired volume porosities, surface porosities, and pore sizes by adjusting the swelling time, swelling temperature, and the type of swelling solvent.

3.3. Surface Properties of the Swelling-Treated SDS Films. We have previously proved that the minority blocks composed of the dispersed phase in BCPs migrate to the film surface and pore wall after selective swelling, changing the surface property of the swelling-treated BCP films.[45] Interestingly, the PDMS block in SDS is more likely to migrate to the film surface because of its lower surface energy compared to that of PS (20.4 vs 40.7 $mN{\cdot}m^{-1}$). Therefore, it is interesting to investigate the surface properties of SDS films before and after swelling in alkanes. XPS was used to monitor the element content on the film surface after swelling in C6 at 25 °C for varied durations. As shown in Figure S6, since silicon only exists in the main chain of PDMS, the content of silicon reflects the relative concentration of the PDMS block on the film surface.

The weight fraction of PDMS in the as-synthesized SDS was estimated to be 15.2 wt %, while the molar fraction was 20.2 mol %. However, the molar fraction of PDMS on the surface of the as-coated SDS film obtained from XPS was determined to be 60.8 mol % (Figure 6a), much higher than that in the bulk SDS copolymer, indicating that a large portion of PDMS has been migrated to the film surface during spin-coating. Such a surface enrichment of PDMS has been commonly reported in other PDMS-containing BCP films.[51] After swelling in C6 for 1 min, the PDMS molar fraction in the film surface decreased to 52.8 mol %, implying the escape of PDMS from the film surface. Remarkably, this is opposite to the progressive migration of the minority blocks to the film surface of amphiphilic BCPs such as PS-*b*-P2VP and PSF-*b*-PEG in selective swelling.[40,45,52−54] We believe this is due to the area where PDMS previously occupies turning into pores (holes) after swelling, thus leading to the declined PDMS content in such a short swelling time. However, prolonging the swelling duration, the surface content of PDMS was increased again as the PDMS blocks continuously migrated to the film surface during swelling. Anyway, because the position of the original PDMS phase has been replaced by pores, the PDMS content on the porous film after swelling still did not exceed that of the pristine film. Moreover, during selective swelling, the PDMS microdomains are swollen and expanded by adsorbing alkanes while the PS phase undergoes plastic deformation, consequently leading to the expansion of film thickness. When the films are removed from the alkane solvents, the alkanes evaporate asynchronously from the less-compatible PS phase and PDMS microdomains; the PS phase accommodating these spaces loses its mobility and serves as the matrix of films promptly, while the PDMS domains remain swollen and mobile until they eventually dry as well. Upon drying, the swollen PDMS chains collapse with the evaporation of alkanes and these spaces occupied by PDMS microdomains change to

https://doi.org/10.1021/acs.macromol.2c01903
Macromolecules 2023, 56, 215−225

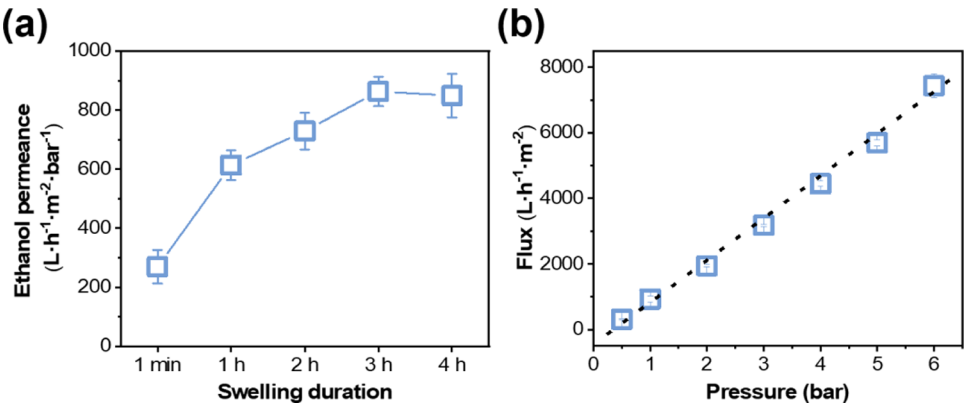

Figure 7. (a) Ethanol permeances of SDS membranes prepared by swelling at room temperature for different durations and (b) ethanol fluxes under various transmembrane pressures of the SDS membrane prepared by swelling at 25 °C for 1 h.

pores. Consequently, the collapsed PDMS chains lined along the film surface and pore walls, endowing the films with inherent hydrophobicity.

The change in WCAs was also investigated to track the swelling process of SDS films swelling in C6 for different durations (Figure 6b). It is worth noting that all of the films exhibited surface hydrophobicity. The WCA of the pristine SDS film before swelling already reached 104.3°, similar to the WCA of PDMS homopolymers,[55] which is a result of the migration of the PDMS blocks to the film surface. Interestingly, although the XPS results revealed a decreased PDMS molar fraction after swelling for 1 min, the WCA of the film was increased to 108.7° instead. WCA depends not only on surface chemistry but also on surface roughness.[56,57] As shown in Figures 6c and S7, due to the low surface energy and the PDMS migration to the film surface during spin-coating, the roughness of the pristine film was extremely low (0.5 nm). However, after swelling for 1 min and 1 h, the roughness was increased to 2.8 and 5.9 nm, respectively. Further prolonging the swelling duration, although the volume porosity and pore size were little changed, the roughness continued to increase, which results in a progressive increase in WCA with swelling duration. Therefore, selective swelling greatly improves the hydrophobicity of the SDS films. After swelling for 4 h, the highest surface roughness of 8.9 nm and WCA of 119.5° indicated that the film has a fairly strong hydrophobicity. Moreover, as shown in Figure 6d, WCAs of SDS films swelling in different alkanes were reduced with the rise of the carbon numbers of the alkanes. This can be easily explained by the decreased surface roughness as a result of a smaller degree of swelling when alkanes with higher carbon numbers were used.

3.4. Permeation of Composite SDS Membranes. By investigating the effects of swelling parameters on the morphology of the SDS films discussed above, we have found that high porosity can be achieved by swelling at room temperature. However, pore accessibility is vital for membrane separation and catalysis applications because liquids cannot pass through blind pores. Therefore, it is necessary to investigate the liquid permeance of the produced nanoporous SDS films to verify whether the pores were interconnected. By spin-coating the SDS solution on the macroporous PVDF substrates followed by selective swelling, composite membranes with the nanoporous SDS films as the selective layers were produced. Due to the hydrophobicity of the SDS films, it was difficult for water to pass through the composite membranes. Hence, we tested the permeance of the membranes using ethanol. The composite membrane, before swelling, gave no permeation to ethanol, indicating that the coated SDS film was dense and defect-free. Despite alcohols have ever been used as selective solvents for PS-based amphiphilic BCPs, they are actually nonsolvents for PS, which can only endow PS with chain mobility at elevated temperatures (e.g., 65 °C) but hardly swell PS at room temperature.[47] Also, we checked the film thicknesses and porosities of SDS films before and after the permeability tests, which hardly changed. Therefore, the shrinkage of SDS films can hardly occur during the permeability tests at room temperature.

After swelling for 1 min, the membrane exhibited an ethanol permeance of 269 $L{\cdot}h^{-1}{\cdot}m^{-2}{\cdot}bar^{-1}$ as a result of pores formed in the SDS coating layer (Figure 7a). The ethanol permeance sharply increased to 613 and 863 $L{\cdot}h^{-1}{\cdot}m^{-2}{\cdot}bar^{-1}$ after swelling for 1 and 3 h, respectively. Further extending swelling to 4 h did not noticeably increase ethanol permeance, which is basically consistent with the evolution of volume porosity with swelling duration shown in Figure 2. The results of ethanol permeance illustrated that although the volume porosity increased rapidly in the early stage of swelling, there were still some pores not penetrative. When the equilibrium swelling is achieved, the surface porosity and pore size hardly change, thus leading to steady ethanol permeance.

We further investigated the pressure resistance of the composite membranes by testing their ethanol flux under different transmembrane pressures. As is shown in Figure 7b, the flux was increased linearly with the pressure increasing from 0.5 to 6.0 bar. No sudden increase or decrease in flux was observed, indicating that the nanoporous SDS layer is robust enough to withstand pressures up to at least 6.0 bar. It should be noted that the pressure resistance of SDS membranes is superior to other PS-based BCP membranes prepared by selective swelling,[41,58,59] which should be ascribed to the enhanced flexibility of the SDS films as a result of the presence of rubbery PDMS.

4. CONCLUSIONS

In summary, we investigate the swelling behaviors of thin films of polystyrene-*block*-poly(dimethylsiloxane)-*block*-polystyrene (PS-*b*-PDMS-*b*-PS, SDS) in linear alkanes with the carbon number increasing from 6 to 10. Alkanes strongly swell PDMS while slightly swell PS, and this difference leads to the cavitation of the PDMS minority phases as a result of selective

https://doi.org/10.1021/acs.macromol.2c01903
Macromolecules 2023, 56, 215−225

swelling-induced pore generation. It is discovered that alkanes with lower carbon numbers as the swelling solvent, longer swelling duration, and higher swelling temperature all result in a stronger swelling effect and, consequently, enlarged pore sizes and porosities. This pore-forming process can be very fast as *n*-hexane is able to produce a porosity as high as 30% at room temperature within 1 min. Thus-produced porous SDS films exhibit strong surface hydrophobicity as a result of the enrichment of PDMS on the film surface. The water contact angle can be enhanced to ∼120° with prolonged swelling duration because of the increased surface roughness. We prove that the films swelling-treated in alkanes have interconnected porosities, which allow the penetration of ethanol with permeation tunable by swelling conditions. The porous SDS films also show good pressure resistance because of the presence of rubbery PDMS. This work reveals the manipulatable interactions between SDS and linear alkanes leading to intriguing compositional and morphological changes on the one hand and provides a nondestructive and facile strategy to prepare hydrophobic nanoporous membranes under mild conditions on the other.

■ ASSOCIATED CONTENT

Supporting Information

The Supporting Information is available free of charge at https://pubs.acs.org/doi/10.1021/acs.macromol.2c01903.

Synthesis route of SDS; ^{1}H NMR spectrogram and TGA curves of SDS; porosities of SDS nanoporous films with long swelling durations; SEM images of porous SDS films; XPS curves of SDS films; and AFM images of SDS films (PDF)

■ AUTHOR INFORMATION

Corresponding Author

Yong Wang − *State Key Laboratory of Materials-Oriented Chemical Engineering, College of Chemical Engineering, Nanjing Tech University, Nanjing 211816 Jiangsu, P. R. China*; orcid.org/0000-0002-8653-514X; Email: yongwang@njtech.edu.cn; Fax: 0086-25-8317 2292

Authors

Shoutian Qiu − *State Key Laboratory of Materials-Oriented Chemical Engineering, College of Chemical Engineering, Nanjing Tech University, Nanjing 211816 Jiangsu, P. R. China*

Zhuo Li − *State Key Laboratory of Materials-Oriented Chemical Engineering, College of Chemical Engineering, Nanjing Tech University, Nanjing 211816 Jiangsu, P. R. China*

Xiangyue Ye − *State Key Laboratory of Materials-Oriented Chemical Engineering, College of Chemical Engineering, Nanjing Tech University, Nanjing 211816 Jiangsu, P. R. China*

Xiang Ying − *State Key Laboratory of Materials-Oriented Chemical Engineering, College of Chemical Engineering, Nanjing Tech University, Nanjing 211816 Jiangsu, P. R. China*

Jiemei Zhou − *State Key Laboratory of Materials-Oriented Chemical Engineering, College of Chemical Engineering, Nanjing Tech University, Nanjing 211816 Jiangsu, P. R. China*

Complete contact information is available at: https://pubs.acs.org/10.1021/acs.macromol.2c01903

Notes

The authors declare no competing financial interest.

■ ACKNOWLEDGMENTS

Financial support from the National Natural Science Foundation of China (21825803, 22108117) is gratefully acknowledged.

■ REFERENCES

(1) Li, C.; Li, Q.; Kaneti, Y. V.; Hou, D.; Yamauchi, Y.; Mai, Y. Self-assembly of block copolymers towards mesoporous materials for energy storage and conversion systems. *Chem. Soc. Rev.* **2020**, *49*, 4681−4736.

(2) Cummins, C.; Lundy, R.; Walsh, J. J.; Ponsinet, V.; Fleury, G.; Morris, M. A. Enabling future nanomanufacturing through block copolymer self-assembly: a review. *Nano Today* **2020**, *35*, No. 100936.

(3) Ruiz, R.; Kang, H.; Detcheverry, F. A.; Dobisz, E.; Kercher, D. S.; Albrecht, T. R.; Pablo, J. J. d.; Nealey, P. F. Density multiplication and improved lithography by directed block copolymer assembly. *Science* **2008**, *321*, 936−939.

(4) Werber, J. R.; Osuji, C. O.; Elimelech, M. Materials for next-generation desalination and water purification membranes. *Nat. Rev. Mater.* **2016**, *1*, No. 16018.

(5) Huang, C.; Zhu, Y.; Man, X. Block copolymer thin films. *Phys. Rep.* **2021**, *932*, 1−36.

(6) Radjabian, M.; Abetz, V. Advanced porous polymer membranes from self-assembling block copolymers. *Prog. Polym. Sci.* **2020**, *102*, No. 101219.

(7) Darling, S. B. Directing the self-assembly of block copolymers. *Prog. Polym. Sci.* **2007**, *32*, 1152−1204.

(8) Ryu, I. H.; Kim, Y. J.; Jung, Y. S.; Lim, J. S.; Ross, C. A.; Son, J. G. Interfacial energy-controlled top coats for gyroid/cylinder phase transitions of polystyrene-block-polydimethylsiloxane block copolymer thin films. *ACS Appl. Mater. Interfaces* **2017**, *9*, 17427−17434.

(9) Kennemur, J. G.; Yao, L.; Bates, F. S.; Hillmyer, M. A. Sub-5 nm domains in ordered poly(cyclohexylethylene)-block-poly(methyl methacrylate) block polymers for lithography. *Macromolecules* **2014**, *47*, 1411−1418.

(10) Ninago, M. D.; Hanazumi, V.; Passaretti, M. G.; Vega, D. A.; Ciolino, A. E.; Villar, M. A. Enhancement of mechanical and optical performance of commercial polystyrenes by blending with siloxane-based copolymers. *J. Appl. Polym. Sci.* **2017**, *134*, No. 45122.

(11) Feng, L.; Fang, H.; Zhou, S.; Wu, L. One-step method for synthesis of PDMS-based macroazoinitiators and block copolymers from the Initiators. *Macromol. Chem. Phys.* **2006**, *207*, 1575−1583.

(12) Yilgör, E.; Yilgör, I. Silicone containing copolymers: Synthesis, properties and applications. *Prog. Polym. Sci.* **2014**, *39*, 1165−1195.

(13) Olson, D. A.; Chen, L.; Hillmyer, M. A. Templating nanoporous polymers with ordered block copolymers. *Chem. Mater.* **2008**, *20*, 869−890.

(14) Jung, Y. S.; Ross, C. A. Orientation-controlled self-assembled nanolithography using a polystyrene-polydimethylsiloxane block copolymer. *Nano Lett.* **2007**, *7*, 2046−2050.

(15) Jung, H.; Shin, W. H.; Park, T. W.; Choi, Y. J.; Yoon, Y. J.; Park, S. H.; Lim, J. H.; Kwon, J. D.; Lee, J. W.; Kwon, S. H.; Seong, G. H.; Kim, K. H.; Park, W. I. Hierarchical multi-level block copolymer patterns by multiple self-assembly. *Nanoscale* **2019**, *11*, 8433−8441.

(16) Son, J. G.; Chang, J. B.; Berggren, K. K.; Ross, C. A. Assembly of sub-10-nm block copolymer patterns with mixed morphology and period using electron irradiation and solvent annealing. *Nano Lett.* **2011**, *11*, 5079−5084.

(17) Nicaise, S. M.; Gadelrab, K. R.; K G, A. T.; Ross, C. A.; Alexander-Katz, A.; Berggren, K. K. Rapid shear alignment of sub-10 nm cylinder-forming block copolymer films based on thermal expansion mismatch. *Nano Fut.* **2017**, *1*, No. 035006.

(18) Lo, T.-Y.; Krishnan, M. R.; Lu, K.-Y.; Ho, R.-M. Silicon-containing block copolymers for lithographic applications. *Prog. Polym. Sci.* **2018**, *77*, 19−68.
(19) Yang, K. C.; Puneet, P.; Chiu, P. T.; Ho, R. M. Well-ordered nanonetwork metamaterials from block copolymer templated syntheses. *Acc. Chem. Res.* **2022**, *55*, 2033−2042.
(20) Cheng, M. H.; Ko, H. W.; Chung, P. Y.; Chang, C. W.; Chen, J. T. Morphology control of three-dimensional nanostructures in porous templates using lamella-forming block copolymers and solvent vapors. *Soft Matter* **2016**, *12*, 8087−8092.
(21) Lin, Y. L.; Cheng, M. H.; Chang, C. W.; Chu, C. W.; Liu, C. T.; Chen, J. T. Curved block copolymer nanodiscs: structure transformations in cylindrical nanopores using the nonsolvent-assisted template wetting method. *Soft Matter* **2019**, *15*, 8201−8209.
(22) Ndoni, S.; Vigild, M. E.; Berg, R. H. Nanoporous materials with spherical and gyroid cavities created by quantitative etching of polydimethylsiloxane in polystyrene-polydimethylsiloxane block copolymers. *J. Am. Chem. Soc.* **2003**, *125*, 13366−13367.
(23) Hansen, M. S.; Vigild, M. E.; Berg, R. H.; Ndoni, S. Nanoporous crosslinked polyisoprene from polyisoprene - polydimethylsiloxane block copolymer. *Polym. Bull.* **2004**, *51*, 403−409.
(24) Guo, F.; Andreasen, J. W.; Vigild, M. E.; Ndoni, S. Influence of 1,2-PB matrix cross-linking on structure and properties of selectively etched 1,2-PB-b-PDMS block copolymers. *Macromolecules* **2007**, *40*, 3669−3675.
(25) Szewczykowski, P. P.; Andersen, K.; Schulte, L.; Mortensen, K.; Vigild, M. E.; Ndoni, S. Elastomers with reversible nanoporosity. *Macromolecules* **2009**, *42*, 5636−5641.
(26) Li, L.; Szewczykowski, P.; Clausen, L. D.; Hansen, K. M.; Jonsson, G. E.; Ndoni, S. Ultrafiltration by gyroid nanoporous polymer membranes. *J. Membr. Sci.* **2011**, *384*, 126−135.
(27) Schulte, L.; Grydgaard, A.; Jakobsen, M. R.; Szewczykowski, P. P.; Guo, F.; Vigild, M. E.; Berg, R. H.; Ndoni, S. Nanoporous materials from stable and metastable structures of 1,2-PB-b-PDMS block copolymers. *Polymer* **2011**, *52*, 422−429.
(28) Guo, F.; Schulte, L.; Vigild, M. E.; Ndoni, S. Load−release of small and macromolecules from elastomers with reversible gyroid mesoporosity. *Soft Matter* **2012**, *8*, 11499−11507.
(29) Lin, T.-C.; Yang, K.-C.; Georgopanos, P.; Avgeropoulos, A.; Ho, R.-M. Gyroid-structured nanoporous polymer monolith from PDMS-containing block copolymers for templated synthesis. *Polymer* **2017**, *126*, 360−367.
(30) Li, T.; Wang, Z.; Schulte, L.; Ndoni, S. Substrate tolerant direct block copolymer nanolithography. *Nanoscale* **2016**, *8*, 136−140.
(31) Li, T.; Wang, Z.; Schulte, L.; Hansen, O.; Ndoni, S. Fast & scalable pattern transfer via block copolymer nanolithography. *RSC Adv.* **2015**, *5*, 102619−102624.
(32) Chao, C.-C.; Wang, T.-C.; Ho, R.-M.; Georgopanos, P.; Avgeropoulos, A.; Thomas, E. L. Robust block copolymer mask for nanopatterning polymer films. *ACS Nano* **2010**, *4*, 2088−2094.
(33) Lo, T.-Y.; Chao, C.-C.; Ho, R.-M.; Georgopanos, P.; Avgeropoulos, A.; Thomas, E. L. Phase transitions of polystyrene-b-poly(dimethylsiloxane) in solvents of varying selectivity. *Macromolecules* **2013**, *46*, 7513−7524.
(34) Wang, Y.; Li, F. An emerging pore-making strategy: confined swelling-induced pore generation in block copolymer materials. *Adv. Mater.* **2011**, *23*, 2134−2148.
(35) Wang, Y.; He, C.; Xing, W.; Li, F.; Tong, L.; Chen, Z.; Liao, X.; Steinhart, M. Nanoporous metal membranes with bicontinuous morphology from recyclable block-copolymer templates. *Adv. Mater.* **2010**, *22*, 2068−2072.
(36) Zhou, J.; Wang, Y. Selective swelling of block copolymers: An upscalable greener process to ultrafiltration membranes? *Macromolecules* **2020**, *53*, 5−17.
(37) Wang, Y. Nondestructive creation of ordered nanopores by selective swelling of block copolymers: toward homoporous membranes. *Acc. Chem. Res.* **2016**, *49*, 1401−1408.
(38) Guo, L.; Wang, Y.; Steinhart, M. Porous block copolymer separation membranes for 21st century sanitation and hygiene. *Chem. Soc. Rev.* **2021**, *50*, 6333−6348.
(39) Yin, J.; Yao, X.; Liou, J.-Y.; Sun, W.; Sun, Y.-S.; Wang, Y. Membranes with highly ordered straight nanopores by selective swelling of fast perpendicularly aligned block copolymers. *ACS Nano* **2013**, *7*, 9961−9974.
(40) Yang, H.; Guo, L.; Wang, Z.; Yan, N.; Wang, Y. Nanoporous Films with Superior Resistance to Protein Adsorption by Selective Swelling of Polystyrene-block-poly(ethylene oxide). *Ind. Eng. Chem. Res.* **2016**, *55*, 8133−8140.
(41) Yang, H.; Lan, Q.; et al. Antifouling ultrafiltration membranes by selective swelling of polystyrene/poly(ethylene oxide) block copolymers. *J. Membr. Sci.* **2017**, *542*, 226−232.
(42) Ahn, H.; Park, S.; Kim, S.-W.; Yoo, P. J.; Ryu, D. Y.; Russell, T. P. Nanoporous block copolymer membranes for ultrafiltration: a simple approach to size tunability. *ACS Nano* **2014**, *8*, 11745−11752.
(43) Zhou, J.; Zhang, C.; Wang, Y. Nanoporous block copolymer membranes immobilized with gold nanoparticles for continuous flow catalysis. *Polym. Chem.* **2019**, *10*, 1642−1649.
(44) Zhang, C.; Yin, C.; Wang, Y.; Zhou, J.; Wang, Y. simultaneous zwitterionization and selective swelling-induced pore generation of block copolymers for antifouling ultrafiltration membranes. *J. Membr. Sci.* **2020**, *599*, No. 117833.
(45) Wang, Z.; Liu, R.; Yang, H.; Wang, Y. Nanoporous polysulfones with in situ PEGylated surfaces by a simple swelling strategy using paired solvents. *Chem. Commun.* **2017**, *53*, 9105−9108.
(46) Brandrup, J.; Immergut, E. H.; Grulke, E. A.; Abe, A.; Bloch, D. R.*Polymer Handbook*; Wiley, 1999.
(47) Zhou, J.; Zhang, C.; Shen, C.; Wang, Y. Synthesis of poly(2-dimethylaminoethyl methacrylate)-block- poly(styrene-alt-N-phenylmaleimide) and its thermo-tolerant nanoporous films prepared by selective swelling. *Polymer* **2019**, *164*, 126−133.
(48) Bussi, Y.; Golan, S.; Dosoretz, C. G.; Eisen, M. S. Synthesis, characterization and performance of polystyrene/PMMA blend membranes for potential water treatment. *Desalination* **2018**, *431*, 35−46.
(49) Soltane, H. B.; Roizard, D.; Favre, E. Effect of pressure on the swelling and fluxes of dense PDMS membranes in nanofiltration: An experimental study. *J. Membr. Sci.* **2013**, *435*, 110−119.
(50) Hansen, C. M.Hansen Solubility Parameters A Users Handbook, 2nd ed.; CRC Press, 2007.
(51) Chen, J.; Gardella, J. A., Jr. Solvent effects on the surface composition of poly(dimethylsiloxane)-co-polystyrene/polystyrene blends. *Macromolecules* **1998**, *31*, 9328−9336.
(52) Wang, Z.; Wang, Y. Highly Permeable and Robust Responsive Nanoporous Membranes by Selective Swelling of Triblock Terpolymers with a Rubbery Block. *Macromolecules* **2016**, *49*, 182−191.
(53) Wang, Z.; Yao, X.; Wang, Y. Swelling-induced mesoporous block copolymer membranes with intrinsically active surfaces for size-selective separation. *J. Mater. Chem.* **2012**, *22*, 20542−20548.
(54) Yan, N.; Wang, Y. Selective swelling induced pore generation of amphiphilic block copolymers: The role of swelling agents. *J. Polym. Sci., Part B: Polym. Phys.* **2016**, *54*, 926−933.
(55) Liu, S.; Zhang, P.; Lü, H.; Zhang, C.; Xia, Q. Fabrication of high aspect ratio microfiber arrays that mimic gecko foot hairs. *Chin. Sci. Bull.* **2012**, *57*, 404−408.
(56) Erbil, H. Y.; Demirel, A. L.; Avcı, Y.; Mert1, O. Transformation of a simple plastic into a superhydrophobic surface. *Science* **2003**, *299*, 1377−13280.
(57) Wang, D.; Sun, Q.; Hokkanen, M. J.; Zhang, C.; Lin, F. Y.; Liu, Q.; Zhu, S. P.; Zhou, T.; Chang, Q.; He, B.; Zhou, Q.; Chen, L.; Wang, Z.; Ras, R. H. A.; Deng, X. Design of robust superhydrophobic surfaces. *Nature* **2020**, *582*, 55−59.
(58) Sun, W.; Wang, Z.; Yao, X.; Guo, L.; Chen, X.; Wang, Y. Surface-active isoporous membranes nondestructively derived from perpendicularly aligned block copolymers for size-selective separation. *J. Membr. Sci.* **2014**, *466*, 229−237.

https://doi.org/10.1021/acs.macromol.2c01903
Macromolecules 2023, 56, 215−225

(59) Shi, X.; Wang, Z.; Wang, Y. Highly permeable nanoporous block copolymer membranes by machine-casting on nonwoven supports: An upscalable route. *J. Membr. Sci.* **2017**, *533*, 201−209.

https://doi.org/10.1021/acs.macromol.2c01903
Macromolecules 2023, 56, 215−225